Research Square

Preprints are preliminary reports that have not undergone peer review.
They should not be considered conclusive, used to inform clinical practice,
or referenced by the media as validated information.

NR3C1/PRKACG-mediated impairment of mitochondrial quality control underlies stress-induced hypothalamic neuronal injury

Weibo Shi

shiweibo@hebmu.edu.cn

Hebei Medical University

Guowei Zhang

Hebei Medical University

Jingze Cong

Hebei Medical University

Xiaowei Feng

Hebei Medical University

Hongjian Xin

Hebei Medical University

Weihao Zhu

Hebei Medical University

Rui Shi

Hebei Medical University

Chenyu Li

Hebei Medical University

Yang Wang

Hebei Medical University

Rufei Ma

Yingmin Li

Bin Cong

Article

Keywords: stress, hypothalamic neuronal injury, mitochondrial quality control, NR3C1, PRKACG

Posted Date: August 11th, 2025

DOI: https://doi.org/10.21203/rs.3.rs-7254381/v1

License: This work is licensed under a Creative Commons Attribution 4.0 International License.
Read Full License

Additional Declarations: There is **NO** Competing Interest.

Version of Record: A version of this preprint was published at Communications Biology on June 4th, 2026. See the published version at https://doi.org/10.1038/s42003-026-10284-y.

Abstract

The hypothalamus integrates autonomic, endocrine, and behavioral responses to stress, and stress-induced hypothalamic neuronal injury is implicated in various diseases. However, the underlying molecular mechanisms remain unclear. Mitochondria, as stress-sensitive organelles, play a critical role in cellular injury through structural and functional alterations. Here, we investigated how stress triggers mitochondrial quality control (MQC) dysfunction via glucocorticoid receptor (NR3C1) signaling, contributing to hypothalamic neuronal injury. Using acute and chronic stress rat models, we demonstrated that stress induces hypothalamic neuronal damage. Transmission electron microscopy and WB analysis revealed that stress promotes excessive mitochondrial fission while suppressing fusion, disrupting mitochondrial dynamics. At the cellular level, ChIP-Seq and siRNA experiments confirmed that glucocorticoids (GCs) downregulate PRKACG expression via NR3C1-mediated transcriptional repression, reducing DRP1 phosphorylation at Ser637 and leading to aberrant mitochondrial fission. Furthermore, acute and chronic stress differentially activate mitophagy pathways, resulting in mitochondrial depletion. Intriguingly, neuronal death shifts from apoptosis to necroptosis under prolonged stress. In conclusion, our findings establish that NR3C1/PRKACG-mediated MQC dysfunction is a key mechanism in stress-induced hypothalamic neuronal injury. This study not only elucidates how GCs disrupt MQC but also advances our understanding of mitochondrial dysregulation in stress-related neuronal damage, providing a foundation for future mechanistic and therapeutic investigations.

Introduction

Stress is a pervasive aspect of daily life, varying in intensity and frequency across individuals[1]. Although responses to stress differ, accumulating evidence indicates that excessive or chronic stress is a major contributor to both physical and mental health disorders. Epidemiological studies have shown that exposure to severe stressors during childhood significantly increases the risk of developing schizophrenia[2]. Moreover, stress is a key precipitating factor in the onset of depression and anxiety disorders. According to a report by the World Health Organization, the global prevalence of anxiety and depression rose by more than 25% in the first year of the COVID-19 pandemic[3]. In addition, stress is strongly associated with the increasing incidence of cardiovascular diseases[4], immune disorders such as rheumatoid arthritis[5], and gastrointestinal conditions[6]. Despite growing recognition of its harmful effects, research into the mechanisms of stress-induced injury remains incomplete. As a result, effective strategies for the prevention and management of stress-related damage are still lacking.

Physiologically, stress activates the sympathetic-adrenomedullary axis and the hypothalamic-pituitary-adrenal (HPA) axis, initiating neural and endocrine responses. The hypothalamus, as the origin of the HPA axis and a key regulator of sympathetic output, orchestrates the release of stress hormones and autonomic reflexes[7]. Upon exposure to stress, hypothalamic neurons become highly active, processing complex signals to coordinate the stress response. This activity demands substantial energy[8], primarily

supplied by mitochondria through oxidative phosphorylation. Mitochondria are not only central to cellular energy production but also act as sensors of internal and external stress signals. Their function is tightly regulated by mitochondrial quality control (MQC), which includes mitochondrial biogenesis, fusion and fission dynamics, mitophagy, and mitochondria- dependent cell death. Dysregulation of MQC has been implicated in neuronal damage across various neuropsychiatric disorders. For instance, increased mitophagy is observed in the cortex and hippocampus of mice with memory impairments[9]. Similarly, activation of the PINK1-Parkin mitophagy pathway is linked to hippocampal neuronal injury following chronic social defeat[10]. In multiple sclerosis, inhibition of necroptosis has been shown to reduce oligodendrocyte loss[11]. In our stress model, we also observed abnormal mitochondrial morphology in neurons, suggesting that mitochondrial dysfunction may contribute to hypothalamic neuronal injury.

Hypothalamic neurons are enriched in glucocorticoid receptors (NR3C1), which mediate negative feedback regulation of glucocorticoids (GC) to maintain homeostasis[12]. However, excessive GC exposure exerts cytotoxic effects[13], damaging hypothalamic neurons and disrupting the regulation of stress hormone secretion and autonomic function. This sustained or excessive GC release perpetuates neuronal injury through NR3C1 signaling, forming a pathological cycle that contributes to systemic dysfunction[14]. Therefore, understanding the molecular mechanisms underlying stress-induced hypothalamic neuronal injury is essential for developing effective interventions. In our restraint stress model, we observed significantly elevated GC levels and increased expression of NR3C1 in the hypothalamus. We hypothesize that stress disrupts MQC via NR3C1, thereby promoting neuronal injury. To test this hypothesis, we conducted an in-depth mechanistic investigation based on our established stress model. These findings aim to inform the development of novel strategies for preventing and treating stress-related injuries.

Results

1. Stress induces damage to hypothalamic neurons.

As the origin of the HPA axis and a key regulatory center of the sympathetic nervous system, the hypothalamus plays a central role in orchestrating the stress response. To investigate the impact of stress on hypothalamic neurons, we established a classical acute and chronic restraint stress model in rats (see Supplementary Fig. 1A). Model validity was confirmed through multiple indicators, including body weight, behavioral assessments (open field and elevated plus maze tests), and fecal pellet output (see Supplementary Fig. 1B–G). With prolonged stress exposure, rats exhibited reduced weight gain, decreased locomotion in the central area of the open field, and significantly lower frequency and duration of entries into the open arms of the elevated plus maze. These changes were accompanied by an increase in fecal pellet output. Collectively, these results indicate the development of anxiety- and depression-like behaviors, confirming successful model establishment. Next, we examined neuronal morphology in the hypothalamus using Hematoxylin-Eosin (HE) and Tar violet staining (Fig. 1A, B). Neurons in acutely stressed rats appeared structurally intact. In contrast, chronic stress induced marked

pathological changes, including tissue edema, neuronal pyknosis, and loss of Nissl bodies. To further assess neuronal integrity, we evaluated the expression of the synaptic protein PSD95 in the hypothalamus (Fig. 1C). Chronic stress significantly reduced PSD95 expression, suggesting progressive synaptic damage with continued stress exposure.

2.Stress induces mitochondrial fission-fusion imbalance.

As mitochondria are sensitive organelles perceiving cellular stress, we first employed transmission electron microscopy to examine the ultrastructural organization of mitochondria in hypothalamic neurons. We observed a clear positive correlation between the duration of stress exposure and mitochondrial damage: with prolonged stress, mitochondria exhibited swelling, fragmentation, cristae disruption and loss, and a significant reduction in mitochondrial volume (Fig. 2A). Mitochondrial morphology is governed by the balance between fission and fusion (literature). Consequently, we systematically assessed the expression changes of key proteins regulating this fission-fusion process. The results indicated that stress significantly activated mitochondrial fission, evidenced by a marked suppression of DRP1 phosphorylation at Ser637 (p-DRP1 Ser637), an increase in DRP1 phosphorylation at Ser616 (p-DRP1 Ser616), and elevated expression of the fission effector FIS1 (Fig. 2B-E). Stress also resulted in a progressive dysfunction of mitochondrial fusion. While the expression of fusion proteins regulating the inner (MFN1 and MFN2)and outer membranes (OPA1) did not exhibit significant changes under acute stress, their expression levels were significantly reduced during chronic stress (Fig. 2F-I). In conclusion, stress induces mitochondrial fragmentation by disturbing the fission-fusion balance. Acute stress mainly activates mitochondrial fission, while chronic stress arises from the persistent hyperactivation of fission coupled with a progressive decline in fusion capacity.

3.The NR3C1–PRKACG axis regulates DRP1 Ser637 phosphorylation and mediates stress-induced mitochondrial fission

To investigate the role of glucocorticoids (GCs) in stress-induced mitochondrial dysfunction, we measured GC levels in serum and glucocorticoid receptor (NR3C1) expression in the hypothalamus. Chronic stress significantly increased both circulating GC levels and hypothalamic NR3C1 expression (Fig. 3A–C). To determine whether elevated GCs contribute to hypothalamic neuronal injury via NR3C1, we established a cortisol-induced cellular stress model in SH-SY5Y cells using 100 μM cortisol. Under this treatment, NR3C1 expression mirrored the in vivo pattern observed in stressed animals (Fig. 3D–F). Next, we employed ChIP-Seq to explore whether NR3C1 mediates transcriptional regulation of mitochondrial fission-related genes. The results showed that cortisol significantly decreased NR3C1 binding to the promoter region of PRKACG, a gene encoding the catalytic subunit of protein kinase A (PKA) (Fig. 3G). PKA phosphorylates DRP1 at Ser637, a modification that inhibits mitochondrial fission. RT-qPCR analysis confirmed that cortisol treatment reduced PRKACG mRNA expression (Fig. 3H). Western blot analysis further demonstrated decreased levels of PRKACG protein and phosphorylated DRP1 at Ser637 following cortisol exposure (Fig. 3I–K). To confirm the involvement of NR3C1, we

silenced its expression using siRNA, achieving approximately 63.7% knockdown efficiency (Fig. 3L). NR3C1 knockdown significantly reversed the cortisol-induced reductions in PRKACG mRNA and protein expression and restored DRP1 Ser637 phosphorylation (Fig. 3M–P). Together, these findings indicate that cortisol suppresses PRKACG transcription through NR3C1-dependent mechanisms, thereby reducing DRP1 Ser637 phosphorylation and promoting excessive mitochondrial fission under stress conditions.

4.Excessive mitochondrial fission activates distinct mitophagy pathways, leading to mitochondrial depletion in hypothalamic neurons

Beyond impairing mitochondrial fusion, excessive fission also promotes mitophagy by generating fragmented mitochondria that serve as substrates for mitophagic clearance. To evaluate mitophagy activation, we measured the levels of LC3-II/I and LAMP1, markers of autophagosome formation and lysosomal activity, respectively. Both acute and chronic stress significantly upregulated these markers, indicating enhanced mitophagy under stress conditions (Fig. 4A–C). To distinguish the mitophagy pathways activated by different stress durations, we further analyzed the expression of key pathway-specific mediators. Acute stress elevated the levels of PINK1 and Parkin, suggesting engagement of the PINK1–Parkin pathway. In contrast, chronic stress induced the expression of BNIP3, BNIP3L, and PINK1, with no significant change in FUNDC1 levels under either condition (Fig. 4D–J). These findings indicate that acute stress primarily activates PINK1–Parkin-mediated mitophagy, whereas chronic stress involves persistent activation of the BNIP3/BNIP3L pathway. To assess mitochondrial biogenesis and overall mitochondrial content, we examined PGC-1α and TOM20 expression in hypothalamic neurons exposed to stress. Both acute and chronic stress suppressed PGC-1α, indicating impaired mitochondrial biogenesis. However, a significant reduction in TOM20 expression—reflecting decreased mitochondrial content—was observed only under chronic stress (Fig. 4K–M).

5.A shift from apoptosis to necroptosis occurs in hypothalamic neurons under acute and chronic stress

As changes in mitochondrial morphology can impair function, we next examined the impact of stress duration on mitochondrial integrity. Both acute and chronic stress increased Cytochrome C (Cyt C) levels (Fig. 5A, B), indicating mitochondrial outer membrane permeabilization. However, only chronic stress significantly reduced mitochondrial membrane potential (ΔΨm), suggesting a decline in mitochondrial function (Fig. 5C, D). Consistent with this, chronic stress markedly elevated reactive oxygen species (ROS) levels (Fig. 5E), further supporting the presence of mitochondrial dysfunction. To explore stress-induced cell death mechanisms, we evaluated mitochondrial-dependent cell death pathways. Acute stress induced significant neuronal apoptosis, whereas chronic stress elicited only a minimal apoptotic response (Fig. 5F). Measurement of intracellular ATP levels revealed that chronic stress substantially

decreased ATP production (Fig. 5G), suggesting impaired energy metabolism. Given that necroptosis is a form of programmed cell death independent of ATP, we investigated the activation of key necroptotic mediators. Acute stress increased RIP1 expression but did not affect RIP3, MLKL, or phosphorylated MLKL at Ser358 (p-MLKL Ser358). In contrast, chronic stress significantly upregulated all these necroptosis-related proteins (Fig. 5H–L), indicating activation of the necroptotic pathway.

6.Inhibition of excessive mitochondrial fission under chronic stress attenuates mitophagy and necroptosis

To elucidate the role of excessive mitochondrial fission in mediating mitophagy, rats exposed to 7 days of restraint stress were treated with the mitochondrial fission inhibitor Mdivi-1 (1.2 mg/kg). Mdivi-1 significantly reduced and improved DRP1 phosphorylation at Ser616 and Ser637 respectively, and restored the expression of mitochondrial fusion proteins MFN1, MFN2, and OPA1 induced by stress (Fig. 6A–F). These findings confirm that Mdivi-1 effectively rebalances the mitochondrial fission-fusion dynamic disrupted by chronic stress. Furthermore, Mdivi-1 treatment markedly attenuated the stress-induced upregulation of mitophagy markers LC3-II/I, LAMP1, and BNIP3/BNIP3L, while also reversing the reduction in TOM20 expression (Fig. 6G–L). These results indicate that suppression of mitochondrial fission mitigates stress-induced mitophagy activation. We next examined whether inhibiting mitochondrial fission also affects necroptosis. Mdivi-1 treatment significantly reduced Cyt C levels, downregulated necroptosis-related proteins, and restored PSD95 expression in the hypothalamus (Fig. 6M–Q), suggesting a rescue of neuronal structural integrity.

Discussion

The hypothalamus, as the central regulator of the body's stress response, plays a crucial role in controlling autonomic, endocrine, and behavioral functions. Structural and functional changes within this region are essential for enabling major organs to respond promptly and effectively to stress. Previous research, including our own, has shown that stress causes dysfunction and injury in hypothalamic neurons[15]; however, the underlying molecular mechanisms remain unclear. To investigate this, we established a rat model combining acute and chronic restraint stress with cold water swimming to simulate varying durations of psychological and physical stress analogous to human conditions. Morphological analysis of this model revealed significant hypothalamic neuronal injury characterized by pyknosis and Nissl body dissolution. Additionally, a pronounced decrease in postsynaptic density protein 95 indicated synaptic impairment. Transmission electron microscopy further demonstrated mitochondrial abnormalities, including cristae dissolution and fragmentation, in hypothalamic neurons following stress. Given mitochondria’s sensitivity to internal and external stressors and their role as the primary energy source for neurons, we hypothesize that stress-induced mitochondrial morphological alterations contribute directly to neuronal damage in the hypothalamus.

Mitochondrial morphology is primarily regulated by the dynamic balance between fusion and fission processes, with mitochondrial function maintained through stringent quality control mechanisms[16]. Fusion involves the merging of the outer mitochondrial membrane, mediated by mitofusin 1 (MFN1) and mitofusin 2 (MFN2), and the inner membrane, facilitated by optic atrophy 1 (OPA1). This process promotes the exchange of mitochondrial DNA, proteins, and metabolites, enhancing cellular adaptability by enabling functional complementation through content mixing[17,18]. Conversely, mitochondrial fission is chiefly controlled by the dynamin-related protein 1 (Drp1) and its receptor Fis1. Cytoplasmic Drp1 undergoes phosphorylation at serine residues 616 and 637, changing the strength of binding to Fis1 on the outer mitochondrial membrane, where it oligomerizes and constricts the membrane to induce division[19]. Notably, phosphorylation at Ser637 and Ser616 has opposing effects: phosphorylation at Ser637 reduces Drp1's GTPase activity and its translocation to mitochondria, thereby inhibiting fission[20]. Balanced fission is essential for the removal of damaged mitochondria and the preservation of cellular homeostasis, while excessive fission leads to cellular injury[21]. Our analysis revealed a significant elevation of mitochondrial fission markers (p-DRP1, Fis1) under acute stress. This effect was further amplified during chronic stress and accompanied by a marked decline in fusion proteins (MFN1, MFN2, OPA1), indicating that stress induces excessive mitochondrial fission and disrupts the fusion-fission equilibrium over time.

Is stress-induced excessive mitochondrial fission linked to elevated glucocorticoid (GC) levels? To explore this, we employed ChIP-seq to examine the interaction between the glucocorticoid receptor (NR3C1) and mitochondrial fission. Notably, we identified, for the first time, that PRKACG—a key regulator of mitochondrial fission—is transcriptionally regulated by NR3C1, a GC-dependent transcription factor. PRKACG encodes a catalytic subunit of protein kinase A (PKA), which phosphorylates DRP1 at Ser637, thereby limiting its translocation to the mitochondrial membrane and inhibiting fission[22]. Following stress exposure, NR3C1 binding to the PRKACG promoter was significantly reduced, suggesting a stress-induced suppression of PRKACG transcription and translation. The resulting decline in PRKACG expression diminishes the inhibition of DRP1-mediated fission, thereby promoting excessive mitochondrial fragmentation. To validate this mechanism, we knocked down NR3C1 expression in cortisol-treated SH-SY5Y cells. Cells transfected with si-NR3C1 exhibited increased PRKACG levels and corresponding reduced mitochondrial fission after cortisol treatment. These findings confirm that the NR3C1-PRKACG signaling axis plays a pivotal role in mediating stress-induced mitochondrial fission in neurons.

Excessive mitochondrial fission promotes mitophagy[23]. Accordingly, we examined mitophagy levels following stress exposure and observed sustained elevations in both mitophagy and lysosomal activity. Combined with a reduction in mitochondrial number, these findings suggest that mitophagy exerts excessive degradative effects post-stress, leading to mitochondrial dysfunction and subsequent neuronal injury—consistent with previous reports[24,25]. In this context, although mitophagy appears to act as a compensatory mechanism during chronic stress, it is insufficient to effectively clear damaged mitochondria. Simultaneously, impaired mitochondrial biogenesis leads to a shortage of functional

mitochondria, exacerbating neuronal damage. Notably, some studies report that glucocorticoid (GC) treatment suppresses mitophagy and compromises its cytoprotective role, potentially due to variations in GC exposure duration, concentration, or the cellular context[26]. Interestingly, we observed a distinct switch in the dominant mitophagy pathway depending on stress duration: the PINK1-Parkin pathway was activated during acute stress, while the BNIP3/BNIP3L pathway became predominant under chronic stress. The PINK1-Parkin axis is considered the canonical mitophagy route, responsible for mitochondrial quality control under physiological conditions[17,27]. In contrast, the BNIP3/BNIP3L and FUNDC1 pathways are typically induced under hypoxic conditions—the former directly regulated by hypoxia-inducible factor 1 (HIF-1), and the latter modulated via oxygen-sensitive kinases[28–30]. Our current investigation did not include detailed assessments of neuronal oxygen metabolism beyond ATP quantification, and the mechanistic basis for this observed pathway switch remains unclear. Could this transition in mitophagy signaling represent a critical determinant in the dual roles—protective versus detrimental—of mitophagy in neurons? Addressing this question will be a central objective of our future studies.

Excessive mitochondrial fission promotes mitophagy, which in turn reduces mitochondrial quality. The decrease in the inner membrane fusion protein OPA1 signifies abnormal inner mitochondrial membrane remodeling[31]. This leads to dysfunctional mitochondria that have undergone excessive fission, causing them to generate more ROS during electron transport, further altering mitochondrial membrane potential, establishing a vicious cycle, and impairing mitochondrial physiological function[32]. Our assessments of JC-1 and ROS also substantiated the loss of mitochondrial membrane function. In line with the increased outer mitochondrial membrane permeability implied by the previously noted reduction in OPA1 protein, the content of the crucial electron carrier Cyt C rapidly increased following stress. Contrary to reports indicating that both BNIP3 and BNIP3L promote Cyt C release[33], we did not observe a further elevation of Cyt C following chronic stress. Accumulated Cyt C leaks from mitochondria into the cytoplasm via compromised mitochondrial membranes, inducing apoptosis[34]. However, TUNEL staining revealed that apoptosis was only significantly elevated during acute stress, which contrasts with the neuronal damage indicated by the reduced PSD95 levels observed under chronic stress conditions. Further analysis revealed a decrease in ATP levels during chronic stress, suggesting that mitochondrial damage within neurons leads to reduced ATP production. This transition from high to low ATP levels shifts the sensitivity of damaged neurons from apoptosis to necroptosis, although the underlying mechanism for this switch remains unclear[35]. Necroptosis is characterized by the partial or complete insertion of MLKL oligomers into the plasma membrane, creating pores or cation channels[36]. This results in the influx of Ca^{2+} and Na^{+}, disruption of osmotic homeostasis, and ultimately culminates in cell lysis and death[37]. The neuronal cell membrane serves as the structural foundation for nerve signal transmission, and this foundation may be compromised by phosphorylated MLKL, thereby accounting for the observed decline in PSD95 levels during chronic stress[38].

Finally, we employed Mdivi-1 to investigate the functional consequences of suppressing stress-induced excessive mitochondrial fission in neurons. We identified an optimal concentration of Mdivi-1 that

selectively inhibited pathological fission without interfering with physiological fission. Interestingly, this dose also reduced mitochondrial fusion, suggesting a regulatory interdependence between these processes. This observation aligns with previous findings, such as those reported by Rambold et al.[39], which demonstrated that enhanced mitochondrial fission can suppress fusion activity. Treatment with Mdivi-1 partially reversed the elevated levels of mitophagy and the reduction in mitochondrial number observed under chronic stress. Additionally, it attenuated the increase in necroptosis and the associated synaptic dysfunction resulting from mitochondrial impairment. These findings suggest that excessive mitochondrial fission heightens the vulnerability of hypothalamic neurons to necroptosis, thereby contributing to neuronal injury.

In conclusion, our study reveals that stress disrupts mitochondrial quality control and induces neuronal damage in the hypothalamus via disinhibition of mitochondrial fission mediated by the NR3C1-PRKACG axis. This pathological process is accompanied by a temporal switch in the dominant mitophagy pathways and a transition in neuronal cell death mode from apoptosis to necroptosis.

Materials and Methods

1. Experimental animals and cell capture

Adult male Sprague-Dawley rats (weighing 200 ± 20g) were obtained from Beijing Vital River Laboratory Animal Technology Co., Ltd. The rats were maintained under controlled conditions: a constant temperature (22 ± 2℃), 50% humidity, and a 12-hour light-dark cycle, with free access to food and water. Following a 7-day acclimatization period in the new environment, the rats were randomly allocated into different treatment groups to establish the stress model. All protocols of the animal experiments have been approved by the Animal Ethics and Welfare Committee of Hebei Medical University (Approval No. IACUC-Hebmu-2023011).

The SH-SY5Y cells (Zhong Qiao Xin Zhou Biotechnology Co., Ltd., ZQ0050) were cultured in complete medium, which is high-glucose DMEM containing 10% fetal bovine serum and 1% penicillin-streptomycin. The cells in complete medium were incubated at 37℃ under a 5% CO_2 atmosphere until reaching 70–80% confluence. Following this, the medium was changed to complete medium containing cortisol at a final concentration of 100 μM, and the cells were incubated for an additional 24 hours to proceed with subsequent experimental procedures.

2. Establishment of the rat stress model

The rats were initially randomized into three groups: the control group (Control), the acute stress group (1d Stress), and the chronic stress group (7d Stress). Rats in the stress groups underwent daily restraint for 6 hours in a transparent acrylic tube, followed by 5 minutes of cold water immersion immediately after release. Control group rats remained in their home cages with food and water deprivation for either 1 or 7 days. The body weight of each rat was recorded prior to the fasting period. For the groups

involving the Mdivi-1 (Mitochondrial division inhibitor 1, MedChemExpress, HY-15886), the chronic stress model was employed. All rats in these four groups were subjected to stereotaxic brain injections before restrained.

3. Stereotactic brain injection

Rats were anesthetized with isoflurane. A burr hole was drilled 1mm posterior and 1.5mm right to the bregma. A guide cannula was implanted into the right lateral ventricle, and drugs were injected into the lateral ventricle at a depth of 4mm. The cannula was secured using stainless steel screws and dental cement. Once the rats recovered from anesthesia, they were returned to their cages for one week of housing before the modeling and drug administration procedures commenced. For the drug dosing, 5% DMSO (TCI, D0798) was prepared in PBS. Mdivi-1 was administered at a dose of 1mg/kg, dissolved in DMSO. Thirty minutes prior to each restraint, the rats were anesthetized with isoflurane and received drug administration through intralateral ventricle injection at a rate of 1 μL/minute.

4. Behavior test

Behavioral tests were performed 24 hours following the establishment of the models in all experimental groups.

Open Field Test: The open field apparatus was a square box constructed from non-toxic, odorless medical-grade acrylic, measuring 100cm × 100cm × 40cm in length, width, and height, respectively. The rats were positioned in the center of the box, facing away from the experimenter, Simultaneously, a video tracking system was initiated to record their locomotor trajectories for 5 minutes. Following the test, the rats were returned to their home cages, and the number of fecal pellets was counted. The interior of the open field box was then sprayed with 75% alcohol to eliminate residual odors that could influence subsequent trials. Once the alcohol had evaporated, the next rat was tested.

Elevated Plus Maze Test: The maze featured two open arms (50cm × 10cm) and two enclosed arms (50cm × 10cm × 40cm), positioned opposite each other and perpendicular, forming a cross. A central platform (10cm × 10cm) was situated at the junction, with the maze elevated 50cm from the floor.Rats were placed in the center of the elevated plus maze facing an open arm, and their activity was monitored by an overhead surveillance camera for 5 minutes. Post-test, the rats were returned to their home cages, and the maze was cleaned with 75% alcohol to prevent residual odors from affecting subsequent trials. Once the alcohol had evaporated, the next rat was tested. Following the completion of behavioral testing, the rats were euthanized under sodium pentobarbital anesthesia. The hypothalamus and abdominal aortic blood were then collected for subsequent experimental procedures.

5. HE and Tar violet staining

Rat brain tissues were fixed in 4% neutral formalin for 36 hours, dehydrated through a graded series of alcohols and xylene, and embedded in paraffin. Subsequently, serial coronal sections (5μm thick) were cut from 7.92 mm to 6.84 mm relative to the interaural line. HE staining: Sections were dewaxed in xylene, rehydrated via a graded alcohol series, stained with hematoxylin for 5 seconds, rinsed in tap water for 5 minutes, differentiated with 0.5% hydrochloric acid ethanol for 3 seconds, and counterstained with eosin for 3 seconds. Tar violet staining: Following dewaxing and rehydration, The sections were immersed in Tar violet staining solution and incubated at 37℃ in an oven for 1 hour. Following rinsing with distilled water to remove excess stain, the sections were immersed in 95% ethanol for differentiation, and the duration of differentiation was adjusted according to the microscopic appearance. The sections were dehydrated through a graded alcohol series, cleared of alcohol using xylene, mounted with neutral resin, and examined under an optical microscope.

6. Western Blot

Protein extraction from the rat hypothalamus was consistently conducted on ice. Tissues were homogenized in RIPA lysis buffer containing protease and phosphatase inhibitors. Following centrifugation at 12,000 rpm for 10 minutes at 4℃, the supernatant was collected as the protein extract. Protein concentration was measured using a BCA Protein Assay Kit. Loading buffer was added in a volume ratio, and the sample was denatured at 95℃ for 10 minutes. Samples were subjected to electrophoresis on 10% or 15% SDS-PAGE gels, and the proteins were transferred onto PVDF membranes that had been pre-activated with methanol using a blotting apparatus. The membrane was incubated with 5% BSA at room temperature for 1 hour to block, followed by incubation with the primary antibody: PSD95 (1:1000, Cell Signaling Technology, #3450), DRP1 (1:1000, Abcam, ab184247), p-DRP1 Ser616 (1:500, Affinity, AF8470)), p-DRP1 Ser637 (1:500, Beyotime, AF5791)), FIS1 (1:1000, Proteintech, 10956-1-AP), MFN1 (1:500, 13798-1-AP), MFN2(1:1000, Proteintech, 12186-1-AP), OPA1 (1:500, Proteintech, 27733-1-AP), NR3C1 (1:1000, Cell Signaling Technology, #3660), PRKACG (1:500,Proteintech, 13697-1-AP), LC3 Ⅰ/Ⅱ (1:500, Cell Signaling Technology, #4108), LAMP1 (1:1000, Abclonal, A16894), PINK1 (1:500, Novus, BC100-494), Parkin (1:100, Abclonal, A0968), BNIP3 (1:500, Abcam, ab109362), BNIP3L (1:500, Cell Signaling Technology, #12396), FUNDC1 (1:5000, Proteintech, 28519-1-AP), PGC-1α (1:500, Abcam, ab191838), TOM20 (1:1000, Abclonal, A6774), Cyto C (1:2000, Abcam, ab133504), RIP1 (1:500, Cell Signaling Technology, #3493), RIP3 (1:500, Santa Cruz, sc-374639), MLKL (1:500, Proteintech, 66675-1-Ig), p-MLKL (1:250, Affinity, AF7420), β-Actin (1:2000, Santa Cruz, sc-47778), GAPDH (1:2000, Report Biotech, RA1005). Antibody diluted in TBST and incubated overnight at 4℃. Following three washes with TBST, the membrane was incubated with the corresponding fluorescent secondary antibody (LICOR, 926-68071; Rockland, 610-145-002; Abbkine, A23710) for 1 hour. After three additional washes with TBST, the membrane was scanned using an Odyssey Dual-color infrared fluorescence imaging system, and band grayscale values were quantified using Image J software.

7. Transmission Electron Microscope (TEM)

Following anesthesia, cardiac perfusion fixation was performed on the rats using 4% paraformaldehyde. After isolation of the hypothalamic tissue, it was trimmed into 1mm × 1mm × 3mm small blocks. These blocks were rapidly placed in 4% glutaraldehyde for fixation and subsequently transferred to the Electron Microscopy Laboratory at Hebei Medical University. The tissue underwent dehydration using acetone at different concentrations. Subsequently, the tissue was embedded in epoxy resin, and mitochondrial morphology was examined under a transmission electron microscope.

8. Enzyme-linked immunosorbent assay (ELISA)

The supernatant of rat blood was obtained following high-speed centrifugation. Pre-treated samples and standards at various concentrations were added to the wells. Horseradish peroxidase-labeled corticosterone was then added, and the plate was incubated at room temperature in the dark for 2 hours. The wells were washed 5 times prior to the addition of TMB. Following a 20-minute incubation, the stop solution was added, and absorbance values were immediately measured using a microplate reader. All experimental procedures were performed strictly according to the manufacturer's instructions for the Corticosterone ELISA Kit (Beyotime, PC100).

9. Cell Counting Kit-8 (CCK8)

SH-SY5Y cells were plated in 96-well plates. The stressed cell model was established as previously described. After modeling, 10 μL CCK-8 solution (Report Biotech, RC3028) was added to each well. The plates were incubated for 1 hour in the incubator, and then the absorbance at 450 nm was measured using a microplate reader.

10. Chromatin immunoprecipitation sequencing (ChIP-Seq)

Upon reaching 70–80% confluence, SH-SY5Y cells were processed using the ChIP kit (Cell Signaling Technology, #9005) to extract and purify chromatin DNA cross-linking with NR3C1 (Cell Signaling Technology, #3660).

The sequencing libraries of immunoprecipitated chromatin DNA were generated with varied index label by NEBNext® UltraTM DNA Library Prep Kit for llumina (NEB, USA, cat. E7645L). Add End Repair Reaction Buffer (10×) and End Prep Enzyme Mix for end repair by the following condition: 20℃ for 30min, 65℃ for 30min. And then NEBNext Adaptor and Blunt/TA Ligase Master Mix was added to ligate adaptor at 20℃ for 15min. USER Enzyme was added to remove base U of adaptor at 37℃ for 5min. After purification with beads, products are amplified with PCR by the following conditions: initial denaturation at 98℃ for 10 sec; denaturation at 98℃ for 10sec, annealing at 65℃ for 30 sec, and extension at 72℃ for 30 sec. The library size was selected and then purified with AMPure XP Beads. Qubit was used for library quantification and High-sensitivity DNA chip was used for test of library insert

size. The libraries were sequenced on an lllumina NovaSeg 6000 platform and 150 bp paired-end reads were generated. Genome data were visualized using the Integrative Genomics Viewer (IGV) software.

11. Transfection of small interfering RNA (SiRNAs)

Upon reaching a 50% confluence of SH-SY5Y cells, the transfection medium was prepared such that each 1mL contained 40 nmol of Si-NR3C1 or Si-NC (Negative Control, obtained from ribobio) and 4μL of HighGene plus Transfection reagent (Abclonal, RM09014P), using the transfection-specific medium (Report Biotech, RE4009). Prior to cortisol treatment, the cells were incubated with the transfection medium for 24 hours. NC: transfection of Si-NC; NCCT: transfection of Si-NC and treated with 100μM cortisol for 24h; NRCT:transfection of Si-NR3C1 and treated with 100μM cortisol for 24h.

12. Real-time fluorescence quantitative polymerase chain reaction (RT-qPCR)

Total RNA was extracted from cell samples of each group via the chloroform extraction method, and its concentration was determined by nucleic acid quantification. Following reverse transcription of RNA into cDNA using Reverse Transcription Mix (Promega, A2791), qPCR was conducted. The reaction system consisted of 2 μL sample, 10 μL qPCR Master Mix (Promega, A6002), 0.4 μL each of forward and reverse primers, and 7.2 μL nuclease-free water. The thermal cycling conditions were as follows: initial denaturation at 95℃ for 1 minute, followed by 45 cycles of 95℃ for 15 seconds and 60℃ for 1 minute. GAPDH served as the internal control, and the relative mRNA expression of the target gene was calculated using the 2-ΔΔCT method.

Primer sequences: NR3C1: Forward: GGAATAGGTGCCAAGGATCTGG, Reverse: GCTTACATCTGGTCTCATGCTGG; PRKACG: Forward: CTGAGCAAAGGCTACAACAAGG, Reverse: GATCTTCTCGTAGATCTGGATGG.

13. Detection of ROS level

Following dissection, the rat hypothalamus was rapidly frozen in liquid nitrogen and subsequently stored at -80℃.The tissue was sectioned into frozen slices (9 μm thick) and then equilibrated to room temperature to manage moisture content. The tissue sections were incubated with an autofluorescence staining agent for 5 minutes, then washed for 10 minutes. The ROS probe (Sigma-Aldrich) was added, and the sections were incubated in the dark at 37℃ for 30 minutes. They were then washed with PBS (pH 7.4) for 5 minutes, three times in total. Finally, an anti-quenching mounting medium containing DAPI was applied. The relative average fluorescence intensity, reflecting ROS levels, was assessed using Image J software.

14. Measurement of mitochondrial membrane potential (JC-1)

Following isolation of the rat hypothalamus, the subsequent steps were performed strictly according to the manufacturer's instructions. Fresh mitochondria were immediately isolated from the hypothalamus using the Tissue Mitochondria Isolation Kit (Beyotime, C3606). An appropriate volume of mitochondrial suspension was added to the JC-1 working solution prepared using the Mitochondrial Membrane Potential Detection Kit (Beyotime, C2005). The fluorescence intensity at various excitation wavelengths was then measured using a fluorescence microplate reader.

15. TUNEL stain

The kit was obtained from ZSGENTECH (ZS-C31009). Following dewaxing and rehydration of the rat brain sections, the experiment was performed strictly according to the manufacturer's instructions. Protease K was added, and the sections were incubated at room temperature for 20 minutes, followed by two PBS washes, each lasting 5 minutes. The pre-prepared TUNEL staining solution was added, and the sections were incubated at 37℃ for 2 hours,. The staining solution was washed off with PBS prior to DAPI counterstaining of the nuclei. Observation was performed using a fluorescence microscope.

16. ATP Content Assay

The ATP Content Assay Kit was obtained from boxbio (AKOP004M). Following the dissection of the rat hypothalamus tissue, the procedure was performed strictly according to the manufacturer's instructions. Following sample extraction and purification, the detection working solution was added sequentially to both the samples and the standards at varying concentrations. Absorbance was measured twice using a microplate reader, and the ATP content of each sample was determined based on the standard curve.

17. statistical analysis

All experiments were performed independently in triplicate or more. Data are presented as the mean ± standard deviation (SD) and were analyzed and graphed using GraphPad Prism 9.5.0. Depending on the experimental group design, t-tests, one-way, or two-way ANOVA were employed for intergroup comparisons. A p-value less than 0.05 was considered statistically significant.

Declarations

Data availability

Uncropped and unedited blot/gel images are available in Supplementary Information. Any remaining information can be obtained from the corresponding author on reasonable request.

Acknowledgements

This work was supported by grants from the Key Projects of the National Natural Science Foundation of China (82130055) and the Major Projects of the National Natural Science Foundation of China (82293651).

Author contributions

G.Z. and J.C. designed and performed the experiments. X.F., H.X., W.Z., R.S. and C.L. recorded data and created the figures. Y.W., R.M. and Y.L. conducted morphological studies. W.S. and B.C. supervised the experimental design and revised the manuscript. All authors have read and agreed to the published version of the manuscript.

Competing interests

The authors declare no competing interests.

Additional information

Supplementary information

References

1. Colombo, D. *et al.* Daily stress encounters: Positive emotion upregulation and depressive symptoms. *Emotion* **24**, 1403-1416 (2024). https://doi.org/10.1037/emo0001362
2. Read, J., van Os, J., Morrison, A. P. & Ross, C. A. Childhood trauma, psychosis and schizophrenia: a literature review with theoretical and clinical implications. *Acta Psychiatr Scand* **112**, 330-350 (2005). https://doi.org/10.1111/j.1600-0447.2005.00634.x
3. Freeman, M. The World Mental Health Report: transforming mental health for all. *World Psychiatry* **21**, 391-392 (2022). https://doi.org/10.1002/wps.21018
4. Vaccarino, V. & Bremner, J. D. Stress and cardiovascular disease: an update. *Nat Rev Cardiol* **21**, 603-616 (2024). https://doi.org/10.1038/s41569-024-01024-y
5. Brock, J. *et al.* Immune mechanisms of depression in rheumatoid arthritis. *Nat Rev Rheumatol* **19**, 790-804 (2023). https://doi.org/10.1038/s41584-023-01037-w
6. Munalisa, R. *et al.* Restraint Stress-Induced Neutrophil Inflammation Contributes to Concurrent Gastrointestinal Injury in Mice. *Int J Mol Sci* **25** (2024). https://doi.org/10.3390/ijms25105261
7. Wei, B. *et al.* Microglia in the hypothalamic paraventricular nucleus sense hemodynamic disturbance and promote sympathetic excitation in hypertension. *Immunity* **57**, 2030-2042 e2038 (2024). https://doi.org/10.1016/j.immuni.2024.07.011
8. Harris, J. J., Jolivet, R. & Attwell, D. Synaptic energy use and supply. *Neuron* **75**, 762-777 (2012). https://doi.org/10.1016/j.neuron.2012.08.019
9. Huang, T. *et al.* Involvement of Mitophagy in Aluminum Oxide Nanoparticle-Induced Impairment of Learning and Memory in Mice. *Neurotox Res* **39**, 378-391 (2021). https://doi.org/10.1007/s12640-

020-00283-0

10. Guo, L. *et al.* Repeated social defeat stress inhibits development of hippocampus neurons through mitophagy and autophagy. *Brain Research Bulletin* **182**, 111-117 (2022). https://doi.org/10.1016/j.brainresbull.2022.01.009
11. Iannielli, A. *et al.* Pharmacological Inhibition of Necroptosis Protects from Dopaminergic Neuronal Cell Death in Parkinson's Disease Models. *Cell Rep* **22**, 2066-2079 (2018). https://doi.org/10.1016/j.celrep.2018.01.089
12. Herman, J. P. *et al.* Regulation of the Hypothalamic-Pituitary-Adrenocortical Stress Response. *Compr Physiol* **6**, 603-621 (2016). https://doi.org/10.1002/cphy.c150015
13. Du, F., Yu, Q., Swerdlow, R. H. & Waites, C. L. Glucocorticoid-driven mitochondrial damage stimulates Tau pathology. *Brain* **146**, 4378-4394 (2023). https://doi.org/10.1093/brain/awad127
14. Shao, W. *et al.* Inhibition of sympathetic tone via hypothalamic descending pathway propagates glucocorticoid-induced endothelial impairment and osteonecrosis of the femoral head. *Bone Res* **12**, 64 (2024). https://doi.org/10.1038/s41413-024-00371-3
15. Zhang, L. *et al.* Interleukin 6 (IL-6) Regulates GABAA Receptors in the Dorsomedial Hypothalamus Nucleus (DMH) through Activation of the JAK/STAT Pathway to Affect Heart Rate Variability in Stressed Rats. *Int J Mol Sci* **24** (2023). https://doi.org/10.3390/ijms241612985
16. Ni, H. M., Williams, J. A. & Ding, W. X. Mitochondrial dynamics and mitochondrial quality control. *Redox Biol* **4**, 6-13 (2015). https://doi.org/10.1016/j.redox.2014.11.006
17. Wang, J. & Zhou, H. Mitochondrial quality control mechanisms as molecular targets in cardiac ischemia-reperfusion injury. *Acta Pharm Sin B* **10**, 1866-1879 (2020). https://doi.org/10.1016/j.apsb.2020.03.004
18. Yang, D. *et al.* Mitochondrial Dynamics: A Key Role in Neurodegeneration and a Potential Target for Neurodegenerative Disease. *Front Neurosci* **15**, 654785 (2021). https://doi.org/10.3389/fnins.2021.654785
19. Cheng, M. *et al.* PGAM5: A crucial role in mitochondrial dynamics and programmed cell death. *Eur J Cell Biol* **100**, 151144 (2021). https://doi.org/10.1016/j.ejcb.2020.151144
20. Liu, B. H. *et al.* Mitochondrial quality control in human health and disease. *Mil Med Res* **11**, 32 (2024). https://doi.org/10.1186/s40779-024-00536-5
21. Dong, W.-T. *et al.* Mitochondrial fission drives neuronal metabolic burden to promote stress susceptibility in male mice. *Nature Metabolism* **5**, 2220-2236 (2023). https://doi.org/10.1038/s42255-023-00924-6
22. Zhu, X. *et al.* Resveratrol prevents Drp1-mediated mitochondrial fission in the diabetic kidney through the PDE4D/PKA pathway. *Phytother Res* **37**, 5916-5931 (2023). https://doi.org/10.1002/ptr.8004
23. Youle, R. J. & Narendra, D. P. Mechanisms of mitophagy. *Nat Rev Mol Cell Biol* **12**, 9-14 (2011). https://doi.org/10.1038/nrm3028

24. Cao, Y. *et al.* A mitochondrial SCF-FBXL4 ubiquitin E3 ligase complex degrades BNIP3 and NIX to restrain mitophagy and prevent mitochondrial disease. *EMBO J* **42**, e113033 (2023). https://doi.org/10.15252/embj.2022113033
25. Ding, W. *et al.* Neuroprotective effects of macrostemonoside T on glutamate-induced injury in HT22 cells. *Biochemical Pharmacology* **235** (2025). https://doi.org/10.1016/j.bcp.2025.116827
26. Choi, G. E. *et al.* BNIP3L/NIX-mediated mitophagy protects against glucocorticoid-induced synapse defects. *Nat Commun* **12**, 487 (2021). https://doi.org/10.1038/s41467-020-20679-y
27. Chen, H. & Chan, D. C. Mitochondrial dynamics--fusion, fission, movement, and mitophagy--in neurodegenerative diseases. *Hum Mol Genet* **18**, R169-176 (2009). https://doi.org/10.1093/hmg/ddp326
28. Hamacher-Brady, A. & Brady, N. R. Mitophagy programs: mechanisms and physiological implications of mitochondrial targeting by autophagy. *Cell Mol Life Sci* **73**, 775-795 (2016). https://doi.org/10.1007/s00018-015-2087-8
29. He, R. *et al.* HIF1A Alleviates compression-induced apoptosis of nucleus pulposus derived stem cells via upregulating autophagy. *Autophagy* **17**, 3338-3360 (2021). https://doi.org/10.1080/15548627.2021.1872227
30. Hui, L. *et al.* Hydrogen peroxide-induced mitophagy contributes to laryngeal cancer cells survival via the upregulation of FUNDC1. *Clin Transl Oncol* **21**, 596-606 (2019). https://doi.org/10.1007/s12094-018-1958-5
31. Giacomello, M., Pyakurel, A., Glytsou, C. & Scorrano, L. The cell biology of mitochondrial membrane dynamics. *Nat Rev Mol Cell Biol* **21**, 204-224 (2020). https://doi.org/10.1038/s41580-020-0210-7
32. Bradford, H. F. *et al.* Thioredoxin is a metabolic rheostat controlling regulatory B cells. *Nat Immunol* **25**, 873-885 (2024). https://doi.org/10.1038/s41590-024-01798-w
33. Liu, J., Wang, J. & Zhou, Y. Upregulation of BNIP3 and translocation to mitochondria in nutrition deprivation induced apoptosis in nucleus pulposus cells. *Joint Bone Spine* **79**, 186-191 (2012). https://doi.org/10.1016/j.jbspin.2011.04.011
34. Bock, F. J. & Tait, S. W. G. Mitochondria as multifaceted regulators of cell death. *Nat Rev Mol Cell Biol* **21**, 85-100 (2020). https://doi.org/10.1038/s41580-019-0173-8
35. Jin, X. *et al.* Therapeutic strategies of targeting non-apoptotic regulated cell death (RCD) with small-molecule compounds in cancer. *Acta Pharm Sin B* **14**, 2815-2853 (2024). https://doi.org/10.1016/j.apsb.2024.04.020
36. Newton, K., Strasser, A., Kayagaki, N. & Dixit, V. M. Cell death. *Cell* **187**, 235-256 (2024). https://doi.org/10.1016/j.cell.2023.11.044
37. Zhou, B. *et al.* Necroptosis Contributes to LPS-Induced Activation of the Hypothalamic-Pituitary-Adrenal Axis in a Piglet Model. *Int J Mol Sci* **23** (2022). https://doi.org/10.3390/ijms231911218
38. Xue, S. G. *et al.* Enhanced TARP-gamma8-PSD-95 coupling in excitatory neurons contributes to the rapid antidepressant-like action of ketamine in male mice. *Nat Commun* **14**, 7971 (2023). https://doi.org/10.1038/s41467-023-42780-8

39. Rambold, A. S., Kostelecky, B., Elia, N. & Lippincott-Schwartz, J. Tubular network formation protects mitochondria from autophagosomal degradation during nutrient starvation. *Proc Natl Acad Sci U S A* **108**, 10190-10195 (2011). https://doi.org/10.1073/pnas.1107402108

Figures

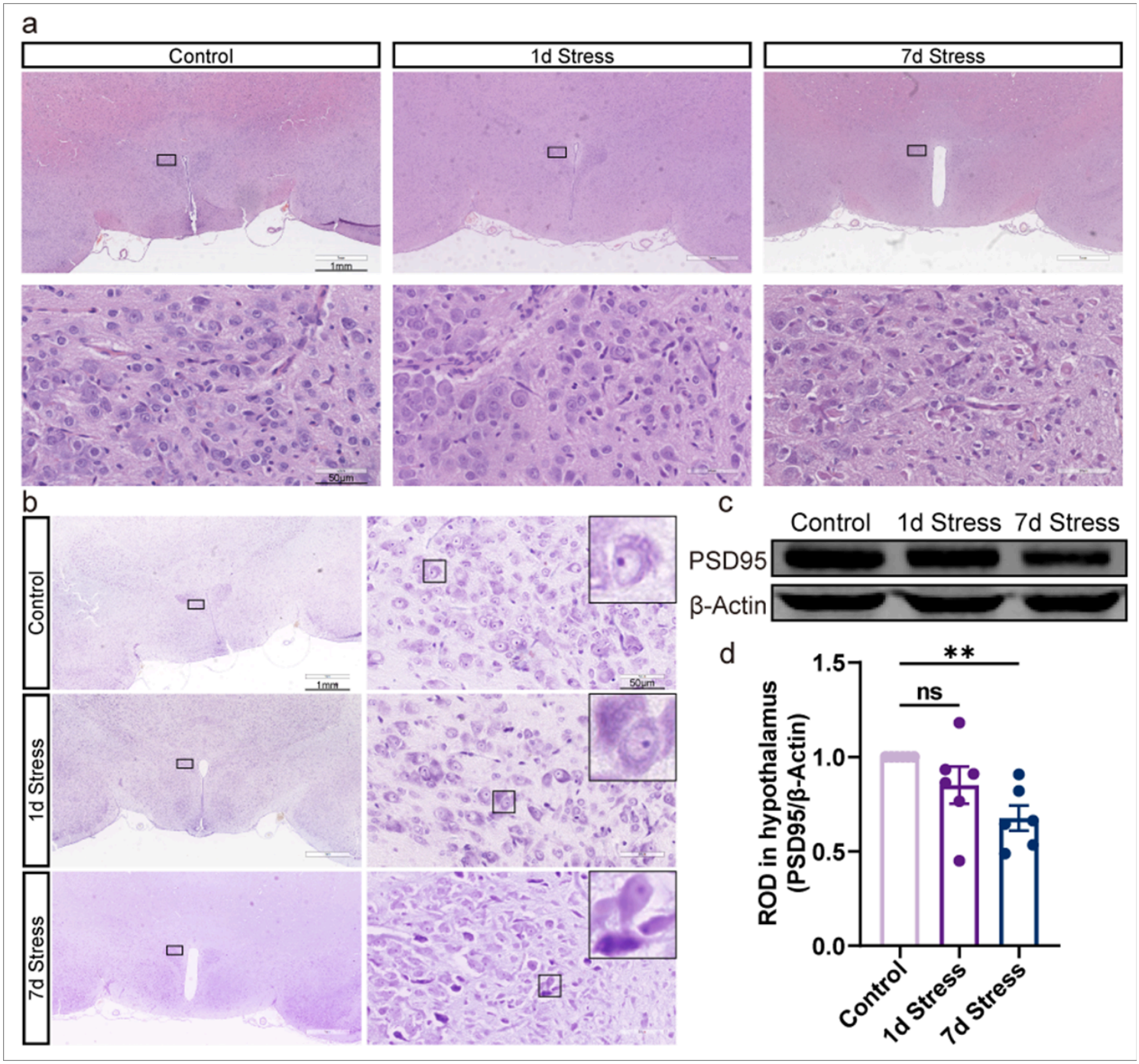


Figure 1

Stress results in alterations in the morphology of hypothalamic neurons and synaptic injury.(A,B) Representative images of HE- and Tar violet-stained rat hypothalamic sections and their corresponding

enlarged views. The length of the scale bar is labeled in the figure. (C,D) PSD95 levels were detected by Western Blot and gray value quantification. One-way ANOVA was conducted. ** indicates $p < 0.01$ versus control.

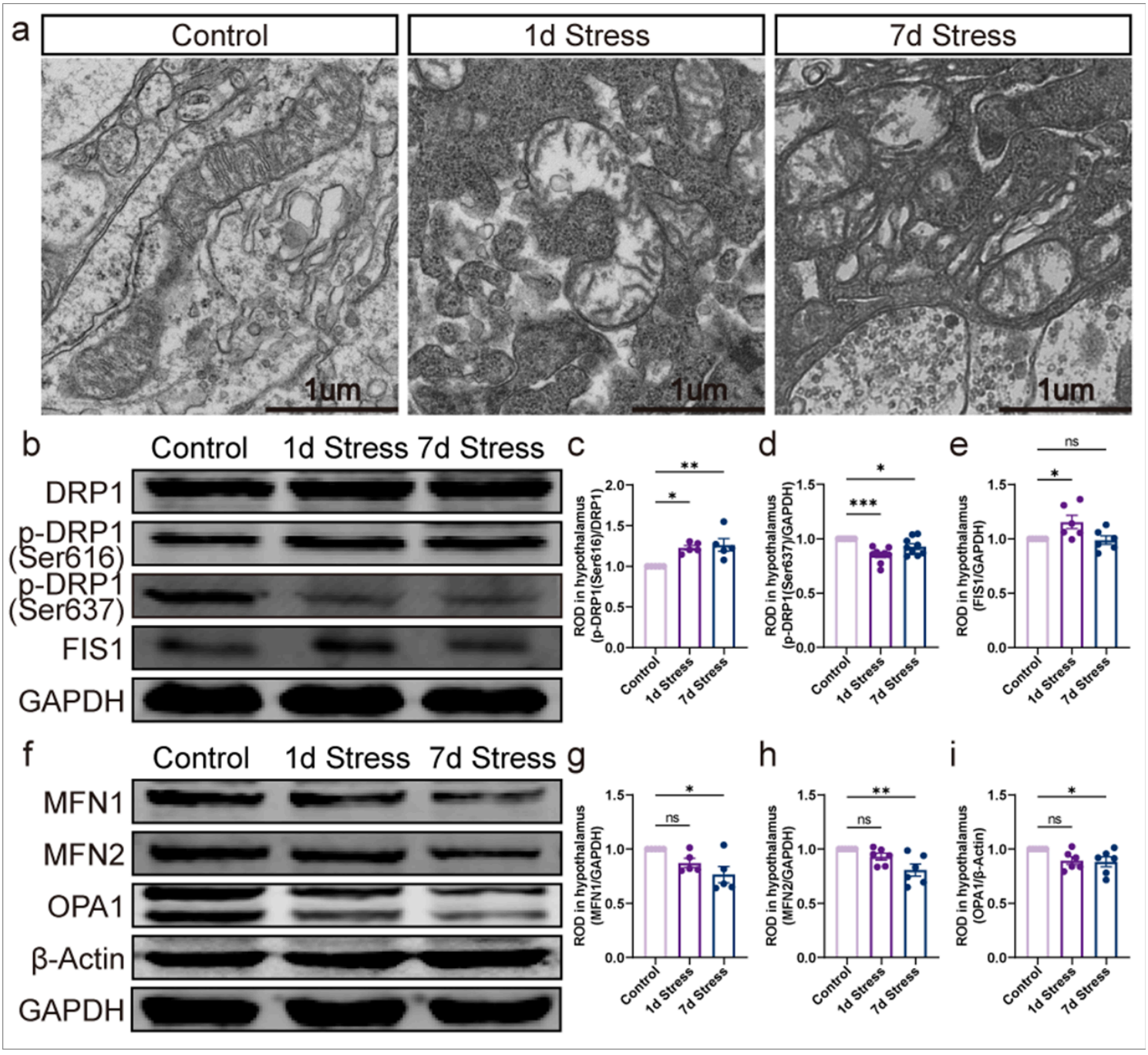


Figure 2

Stress results in mitochondrial hyperactive fission and hypoactive fusion. (A) Representative images of TEM from different groups. (B-E) Western blot images and densitometric quantification of mitochondrial fission related protein DRP1, p-DRP1 (Ser616), p-DRP1 (Ser637) and FIS1 in the hypothalamus. (F-I) Western blot images and densitometric quantification of protein related to mitochondrial fusion MFN1,

MFN2 and OPA1 in the hypothalamus. One-way ANOVA was conducted. *,**,*** indicates $p < 0.05$, $p < 0.01$, $p < 0.001$ versus control, respectively.

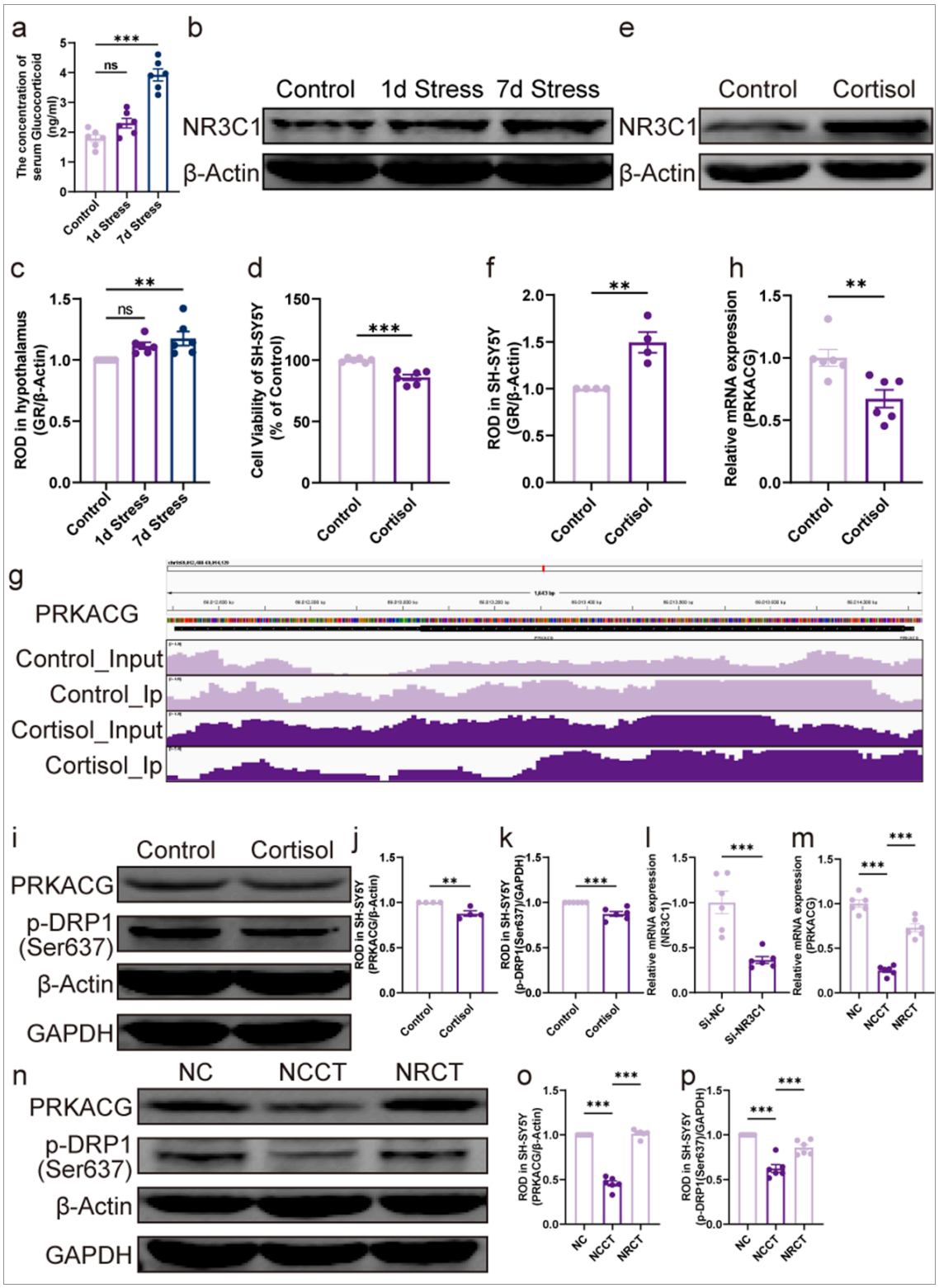


Figure 3

NR3C1-dependent transcriptional inhibition of PRKACG leads to excessive mitochondrial fission.(A) The concentration of GC level in the serum. (B,C) Representative images of Western Blot of NR3C1 and

its quantification in rat hypothalamus. (D) The bar chart of CCK-8 after 100μM cortisol administration for 24h. (E,F) Representative images of Western Blot of NR3C1 and its quantification in SH-SY5Y. (G) The igv visualization of reads alignment results of PRKACG in ChIP-Seq data. (H) The relative quantification of PRKACG mRNA expression in SH-SY5Y. (I-K) Representative images of Western Blot of PRKACG and p-DRP1 (Ser637), and the quantification in SH-SY5Y. (L) The relative quantification of NR3C1 mRNA expression in SH-SY5Y after transfection of siRNAs. (M) The relative quantification of PRKACG mRNA expression in SH-SY5Y after transfection of siRNAs. (N-P) Representative images of Western Blot of PRKACG and p-DRP1 (Ser637), and the quantification in SH-SY5Y after transfection of siRNAs. T test or one-way ANOVA was conducted. *,**,*** indicates $p < 0.05$, $p < 0.01$, $p < 0.001$ versus control, respectively.

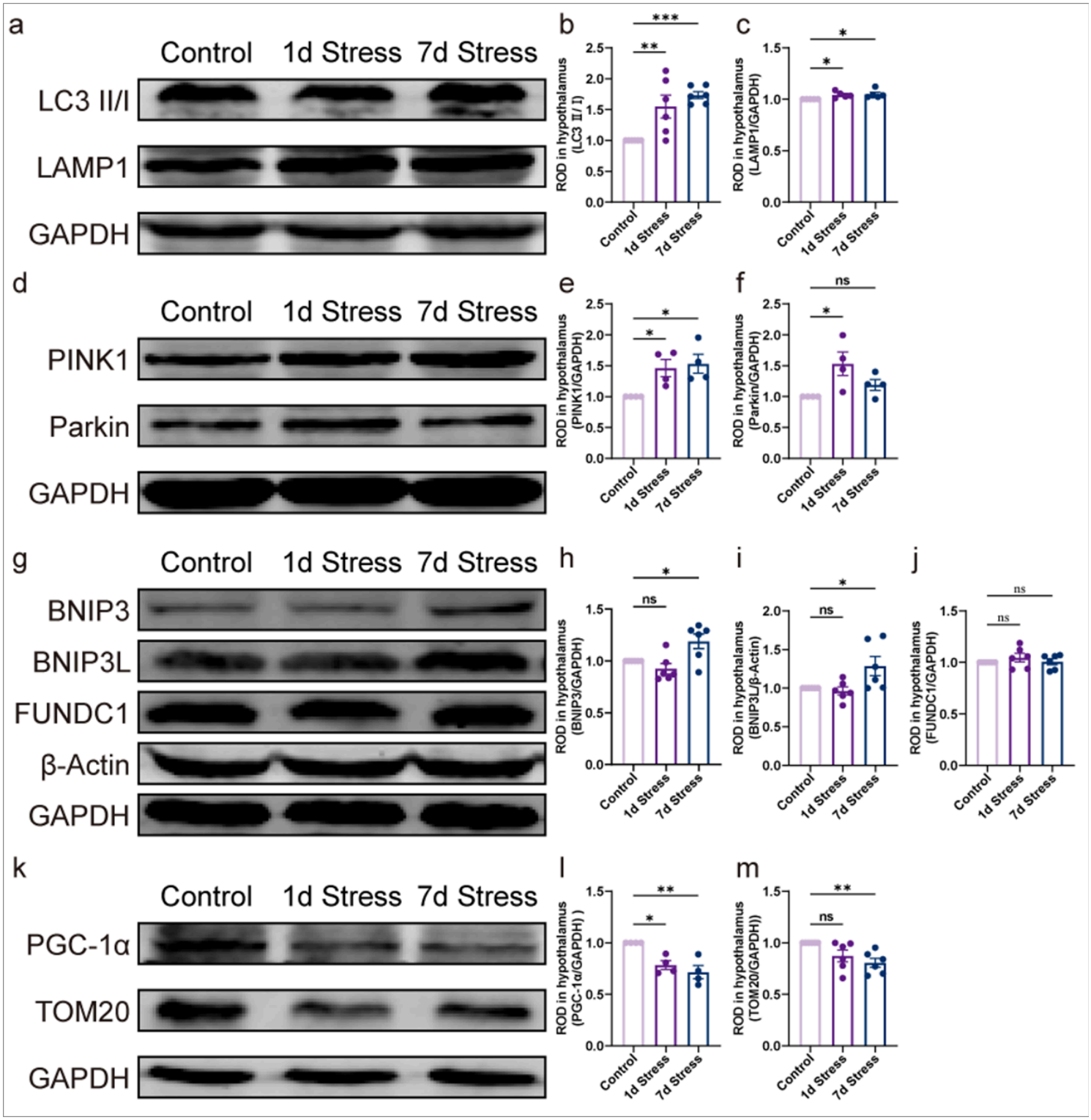


Figure 4

Hyperactivated mitophagy and decreased mitochondrial biogenesis result in mitochondrial exhaustion. (A-C) Representative images of Western Blot of LC3 Ⅱ/Ⅰ and LAMP1, and the quantification in rat hypothalamus. (D-E) Western blot images and densitometric quantification of mitophagy related protein PINK1 and Parkin in the hypothalamus. (G-J) Western blot images and densitometric quantification of mitophagy related protein BNIP3, BNIP3L and FUNDC1 in the hypothalamus. (K-M) Representative

images of Western Blot of PGC-1α and TOM20, and the quantification in rat hypothalamus. One-way ANOVA was conducted. *,**,*** indicates $p < 0.05$, $p < 0.01$, $p < 0.001$ versus control, respectively.

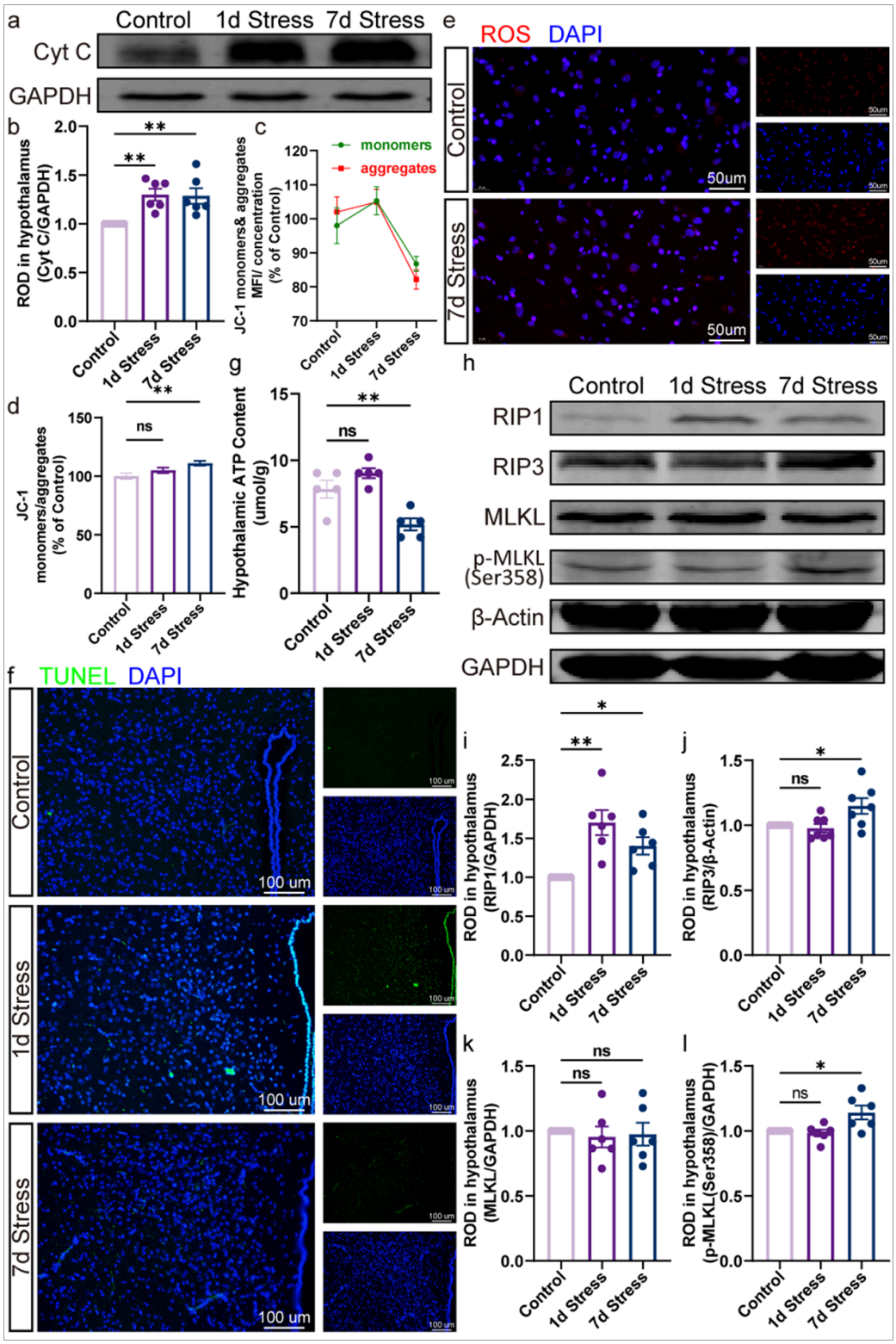


Figure 5

Neuronal injury following chronic stress is mediated by necroptosis. (A,B) Representative images of Western Blot of Cyt C and its quantification in rat hypothalamus. (C,D) The membrane potential detection

of mitochondria (JC-1) in rat hypothalamus. The line graph illustrates the ratio of the mean fluorescence intensities of two types to the mitochondrial protein mass. The bar graph shows the ratio of monomers to aggregates fluorescence intensities for each individual sample. (E) Detection of ROS level in the rat hypothalamus, and their corresponding enlarged views are on the right. (F) TUNEL assay of rat hypothalamic sections. The picture on the right is a magnified view. (G) ATP content assay of the rat hypothalamus. (H-L) Western blot images and densitometric quantification of necroptosis related protein RIP1, RIP3 MLKL and p-MLKL (Ser358) in the hypothalamus. The length of the scale bar is labeled in the figure. One-way ANOVA was conducted. *,**,*** indicates $p < 0.05$, $p < 0.01$, $p < 0.001$ versus control, respectively.

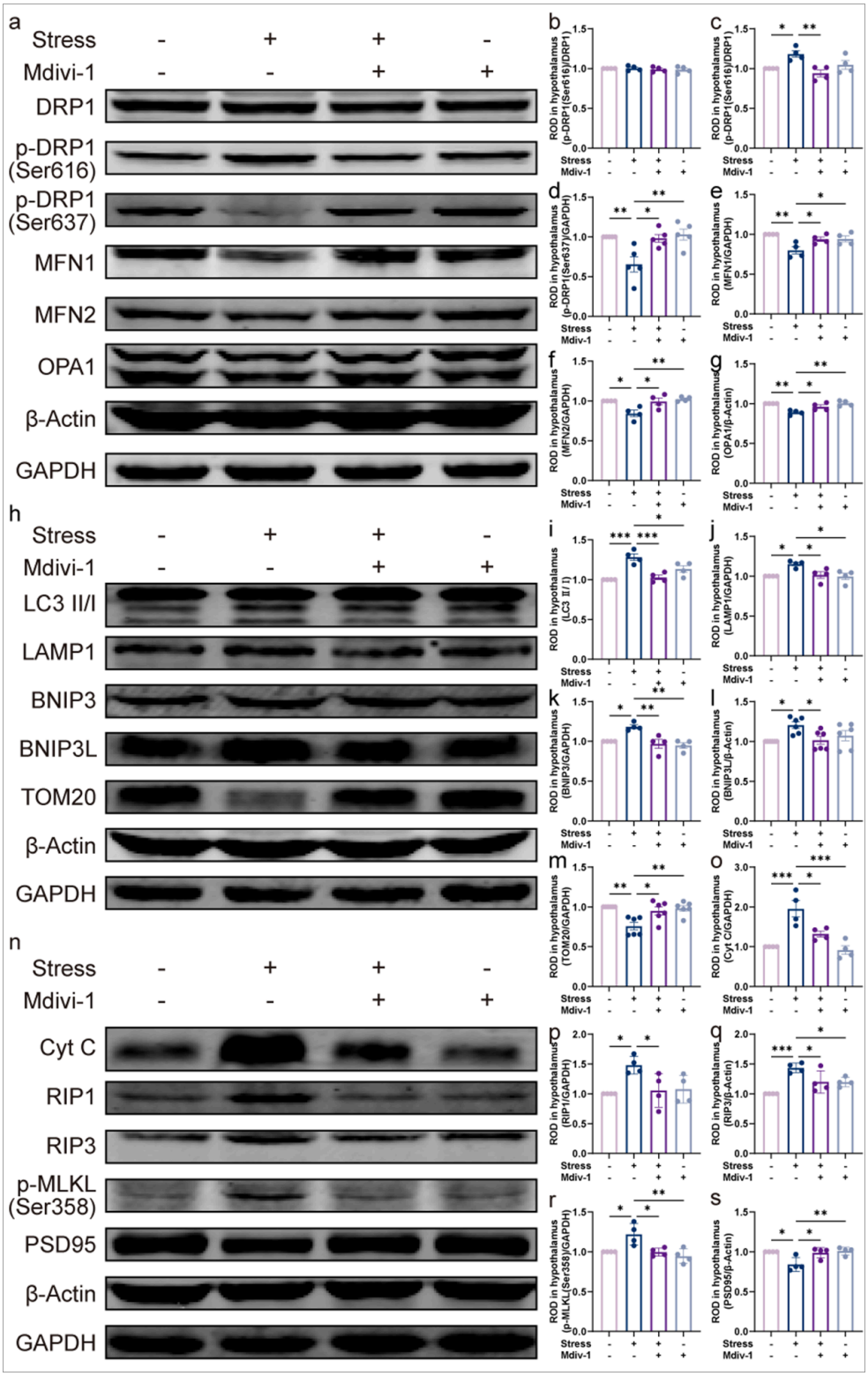


Figure 6

Mitochondrial fission induces excessive mitophagy and necroptosis following chronic stress.(A-F) Representative images of Western Blot of DRP1, p-DRP1 (Ser616), p-DRP1 (Ser637) , FIS1 , MFN1, MFN2 and OPA1, and the quantification in the hypothalamus. (G-L) Representative images of Western Blot of LC3 Ⅱ/Ⅰ , LAMP1, PINK1, Parkin, BNIP3, BNIP3L and TOM20, and the quantification in the hypothalamus. (M-Q) Representative images of Western Blot of Cyt C , RIP1, RIP3 and p-MLKL (Ser358) , and the

quantification in the hypothalamus. Two-way ANOVA was conducted. *,**,*** indicates $p< 0.05$, $p < 0.01$, $p < 0.001$ versus control, respectively.

Supplementary Files

This is a list of supplementary files associated with this preprint. Click to download.

- Supplementaryinformation.pdf